On the rejection and reversibility of fouling in ultrafiltration as assessed by hydraulic impedance spectroscopy

M.C. Martí-Calatayud[a,b], S. Schneider[a], M. Wessling[a,c,*]

[a]*RWTH Aachen University, Chemical Process Engineering, Forckenbeckstr. 51, 52074 Aachen, Germany*
[b]*Universitat Politècnica de València, IEC Group, Departament d'Enginyeria Quimica i Nuclear, Camí de Vera s/n, 46022, València, Spain*
[c]*DWI Interactive Materials Research, Forckenbeckstr. 50, 52074 Aachen, Germany*

Abstract

The manifestation of critical fluxes in membrane filtration has typically served to set an upper value above which detrimental fouling events and a substantial increase of membrane resistance occurs. Despite the usefulness of critical flux concepts for conducting sustainable membrane processes, the specific phenomena causing them cannot be easily identified via conventional membrane filtration modes. Usually arbitrary fouling rates are selected to delimit the boundary between under- and over-critical flux operation. Timescales respective for colloidal matter accumulation are overlooked.

Frequency response analysis of transmembrane pressures has been recently presented as a highly-sensitive method to track fouling in ultrafiltration. This hydraulic impedance spectroscopy method allows not only measuring membrane resistances but also corresponding time constants related to

*Corresponding author
Email addresses: `mamarc13@upvnet.upv.es` (M.C. Martí-Calatayud),
`manuscripts.cvt@avt.rwth-aachen.de` (M. Wessling)

colloidal matter accumulation. In this work, hydraulic impedance spectra are gained for the ultrafiltration of different model foulants to assess the origin of critical fluxes for two different membranes. A correlation among characteristic impedance features and the type of fouling could be established: the evolution of phase shift between flux and pressure at increasing fluxes allows identifying the formation of external fouling layers, while registering of hysteresis loops at reversed frequency sequences signals the development of irreversible internal fouling. The hydraulic impedance method emerges as a precise and more sensitive monitoring tool to diagnose the beginning and nature of critical fouling.

1. Introduction

Membrane processes are mainly evaluated based on the membranes' capacity to permeate desired products and reject unwanted components present in a feed stream. Additionally, technical parameters necessarily influence the membrane lifespan, the frequency of required cleanings and the energy input that is needed to achieve a certain separation performance [1–3]. Such parameters enclose aspects like membrane structure and material, its propensity to foul, membrane-foulant interactions or the operation modes and conditions.

Membrane characterization methods are principally based on conducting plain permeation experiments to analyze the feed, retentate and permeate

2

streams and to obtain the relationship between permeate flux and transmembrane pressure (TMP). Both parameters are usually represented in fouling curves composed of two regions of different membrane behavior which are well differentiated. At low transmembrane pressures, permeate flux increases linearly with pressure. However, when the permeate flux is increased reaching a certain level, solutes are more difficultly removed from the membrane surface back to the bulk solution by means of convection and back-diffusion. More colloidal matter settles on the membrane surface or within the pores, decreasing the permeability; the resistance of accumulation layers becomes process-limiting and the permeate flux can be hardly increased. The flux at which the transition between pressure-dependent and pressure-independent flux behavior takes place is usually known in the literature as critical flux and was initially modelled by Bacchin et al. and formulated by Field et al. [4, 5]. The first definitions were based on the calculation of repulsive forces between solutes and a permeable surface, so that the critical flux was related to the attainment of an equilibrium where the repulsive forces between both are overcome and from which the deposition of material at the membrane surface starts to occur. A recent simulation work showed that microscopic events taking place at the inner pore geometry, whose nature is yet unexplored, also determine colloidal matter deposition [6]. Determining critical fluxes and getting knowledge on the nature of fouling causing them is highly relevant for practical applications of membrane processes, as operating under conditions which minimize or delay fouling development contributes to ensure a long-lasting and sustainable process performance and to reduce operating costs.

3

After the introduction of the term critical flux a variety of more specific types and definitions of characteristic fluxes have emerged over time, e.g. threshold flux, 'strong' and 'weak' form of critical flux, etc. These have been deeply reviewed and summarized in different works [7–9]. Espinasse et al. developed a square-wave pressure method to distinguish between the dispersed accumulation of colloids and the irreversible condensation of matter on the membrane surface [10]. In the same line, a so-called 'improved flux-step method' was established, from which TMP profiles registered during intermediate relaxation steps were used to calculate the critical flux for irreversibility, which was defined as the flux where fouling cannot be removed by intermediate physical cleaning techniques [11]. Since fouling already takes place at permeate fluxes below the critical one, the term sustainable flux has been introduced in the last years in order to distinguish between filtration at low fouling and high fouling rates [8]. Above sustainable flux conditions severe and fast-developing fouling takes place, hence leading either to frequent cleaning cycles or to accelerated membrane deterioration.

Besides the numerous nomenclatures and definitions of characteristic fluxes, the type of measurement methods employed for their determination vary significantly within the literature. Usually flux- or pressure-stepping methods are implemented in different forms for determining fouling rates and critical fluxes. The choice of the parameters of stepping methods is usually subjective, while the criteria for determining characteristic fluxes are normally based on arbitrary considerations about a specific $dTMP/dt$ rate [12–14].

4

Among others, the range of feed mixtures and membrane systems analyzed make even more difficult establishing a standardized measuring procedure for the determination of characteristic fluxes and to interpret the main phenomena originating them [8]. Particularly, one must take into account that membrane filtration is a dynamic process where fouling is being measured and, at the same time, evolving during the course of the measurement. In an important review, Bacchin et al. emphasized the relevance of timescales employed in membrane characterization measurements and proposed the utilization of the dimensionless Deborah number for colloidal stability, in order to account for timescale effects specially when the coagulation of a suspension on a membrane occurs very slowly [9]. The Deborah number, D_m, is defined as the ratio between the time for coagulation on the membrane and the time of observation. Accordingly, at D_m values higher than one important accumulation effects might be underestimated during the membrane characterization.

In our previous publication a novel method for characterizing membrane systems which takes into account relaxation times of colloidal accumulation was presented [15]. In contrast with pressure- or flux-stepping protocols, the developed method, called hydraulic impedance spectroscopy, is based on a frequency response analysis of TMP signals at a constant flux. In hydraulic impedance spectroscopy a constant average flux is applied, to which an oscillating signal with the shape of a sine function is summed. The period of the sinusoidal perturbations is varied during the measurement, so that evolution of fouling is analyzed at different timescales. The hydraulic resistance

5

of the system is thus calculated from the relationship between TMP and permeate flux signals at each frequency. At the limit of frequencies tending to zero, all phenomena involved in the filtration process have enough time to fully develop; consequently, their contribution to the overall system response is comprised in the impedance spectra. The timely evolution of accumulation processes can be thereupon evaluated by analyzing the evolution of impedance spectra when registered from high to low frequencies. In addition to the analysis of complex hydraulic resistances, the accumulation of colloidal matter at the feed side of the membranes induces a dispersion between TMP and permeate flux which fingerprints the properties of the deposition layer.

In the present study, hydraulic impedance spectroscopy measurements are conducted with a combination of different membranes and colloidal solutions. First, we demonstrate that hydraulic impedance spectra can simultaneously provide information on the selective properties and on the hydraulic resistance of a membrane system. After screening the membrane behavior by means of flux step methods, the impedance response of each investigated system is obtained at different average flux levels. Special focus is put on the transition between membrane resistance-limited behavior (at under-critical fluxes) and fouling resistance-limited behavior (near the critical flux). The main objective of this work is to use the superior sensitivity of hydraulic impedance measurements to precisely identify the flux at which critical fouling starts to develop. The nature of fouling is also tracked by evaluating the evolution of impedance spectra as the average permeate flux is increased. In this respect, a correlation between different characteristic impedance fea-

tures and the type of fouling being analyzed is assessed in order to identify the occurrence of irreversible colloidal matter deposition in the membrane. We hypothesize and prove below that the hydraulic impedance analysis facilitates the distinction between external gel layer formation and internal and irreversible pore clogging in different membrane systems.

2. Theory

Impedance studies have been widely conducted in the field of electrical engineering and electrochemistry. They are based on the perturbation of a system with a periodic sinusoidal signal of small amplitude and the measurement of a response variable. When the signal is applied at different frequencies, the method receives the name of impedance spectroscopy. In electrochemical systems, usually an input potential is given and the current response is measured. In contrast to steady-state measurements, where the calculation of the overall system resistance is the main objective of the experiment, impedance measurements are based on analyzing dynamic responses in the frequency domain to obtain information on distinct phenomena predominating at different timescales and contributing to the system response. The benefit of impedance measurements lies on the fact that systems usually offer a more complex behavior than a perfect resistor. For example, capacitive and inductive components of a system response can be accessed from dispersions arising between current and voltage at certain frequencies [16–18].

In the case of hydraulic (also called fluidic) impedance spectroscopy, whose analogy with the electrochemical impedance spectroscopy was ex-

7

plained in detail in a previous publication [15], the complex hydraulic resistance of a membrane system, Z_H (mbar/($L \cdot m^{-2} \cdot h^{-1}$) or mbar/LMH), can be defined as the ratio between the transmembrane pressure and flux:

$$Z_H = \frac{TMP}{j_p}$$

(1)

Where TMP (mbar) represents the transmembrane pressure and j_p (LMH) the permeate flux. Let us introduce a perturbation in the permeate flux with a sinusoidal shape:

$$j_p(\omega t) = j_{p,0} \cdot sin(\omega t)$$

(2)

Where $j_{p,0}$ is the amplitude of the permeate flux and ω is the angular frequency of the sine function. ω is a function of the frequency f, where $\omega = 2\pi f$. In the case of a quasi-linear behavior of the system, which occurs when the amplitude of the perturbation is rather small, TMP should respond also with a sinusoidal shape, being described by an equation taking the following form:

$$TMP(\omega t) = TMP_0 \cdot sin(\omega t + \varphi)$$

(3)

where TMP_0 and φ represent the amplitude of the TMP signal and the phase shift between TMP and j_p signals, respectively. If the frequency-dependent expressions for both variables are then substituted in Eq. (1), after applying some trigonometric transformations we obtain:

8

$$Z_H(\omega) = \frac{TMP_0}{j_{p,0}} \cdot (cos \ \varphi + j \cdot sin \ \varphi) \tag{4}$$

In the previous equation j represents the imaginary unit. As seen from the above equation, the hydraulic impedance takes the form of a complex number, which can be expressed as the sum of a real and an imaginary part:

$$Re \ Z_H(\omega) = |Z_H| \cdot cos \ \varphi \tag{5}$$

and

$$Im \ Z_H(\omega) = |Z_H| \cdot sin \ \varphi \tag{6}$$

The modulus of the impedance $|Z_H|$ takes the form of:

$$|Z_H| = \frac{TMP_0}{j_{p,0}} \tag{7}$$

The most common forms of representing impedance data are Nyquist and Bode plots. A scheme illustrating the construction of both types of graphical representations from raw experimental data is shown in Fig. 1. The figure shows the typical response obtained for ultrafiltration membranes during the filtration of colloidal solutions [15]. The amplitudes of permeate flux and transmembrane pressure, as well as the phase shift between both signals obtained at every probed frequency are the basis for the calculation of the

9

hydraulic impedance. In Nyquist plots, the negative imaginary component of Z_H is plotted against the real one in a complex-plane diagram. $Re\,Z_H$ is representative for the resistive behavior of the system. In other words, it provides a measure of the hydraulic resistance of the system. $Im\,Z_H$ is a measure of the capacitance of the system. In fluidic systems, the capacitance is termed compliance and indicates how much matter is accumulated in the investigated control volume upon a variation in pressure, dm/dp [19–21]. At frequencies where both TMP and $j_{p,0}$ are in phase, the values of $Im\,Z_H$ become zero and the system behaves as an ideal resistor. This occurs at the limits when the frequency approaches 0 and ∞. The value of $Re\,Z_H$ at the limit of very low frequencies can be considered as the inverse of the membrane permeability, which corresponds to the steady state of the system. At intermediate frequencies, the dispersion between TMP and j_p is more notorious, that is, compliant effects can be usually identified when sine-wave signals of intermediate frequency are applied. Finally, at the limit of very high frequencies the amplitude of the response signal does not have enough time to develop and, consequently, the impedance takes a value of zero. The semicircle shape in Nyquist diagrams is representative of systems with a single time constant, which in the present case is associated with the deposition of colloidal matter in the membrane.

Bode diagrams are representations of $log\,|Z_H|$ and φ against the logarithm of the frequency; consequently, they provide explicit information about the probed frequencies. When a system whose behavior is assumed to be represented by a compliance and a resistance in parallel, the Bode magnitude plot

10

shows two linear regions: one at low frequencies approaching the inverse of membrane permeability, and the other one at very high frequencies showing decreasing values of $log\,|Z_H|$.

200

Diagrams as those exemplary shown in Fig. 1 allow obtaining the characteristic relaxation times of the process of colloidal matter accumulation in a membrane. Time constants basically indicate how fast a system reacts upon a perturbation until reaching a new steady state. They can be identified in the Nyquist diagram from the inverse of the frequency at which the maximum in $Im\,Z_H$ is registered, or alternatively, from the break-point in the Bode diagram.

3. Experimental

Two different filtration setups were used for conducting the impedance measurements (Fig. 2). A crossflow module was used for the filtration of dextran solutions, which were carried out to characterize the rejection and molecular weight cut-off (MWCO) of the membranes. The effective membrane area used in this module was 93.5 cm^2. Compared to the other submerged filtration modules used in the present work, this setup can be operated at a wider range of positive pressures, thus allowing the utilization of high concentrations of dextrans. Samples taken during the experiments can be directly analyzed by size exclusion chromatography (SEC) and the high permeate fluxes achieved with this configuration also ensure an accurate measurement of the hydraulic impedance. This system uses two different
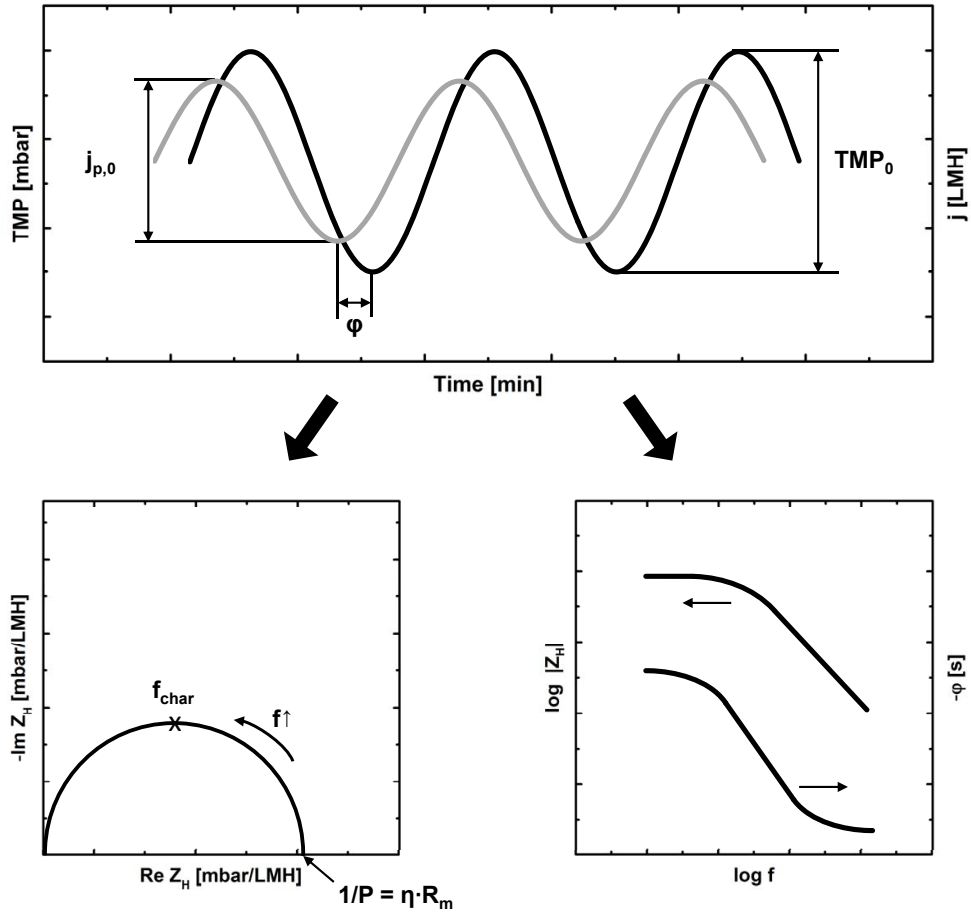
11

Figure 1: Measurement of hydraulic impedance and its graphical representation.

pumps: one pump (P-1, Ismatec Reglo) is used to implement a sinusoidal signal in the permeate flux, and a second one (P-2, Ismatec MCP-Z) is used as feed/retentate pump to achieve sufficiently high transmembrane pressures and crossflow rates. The pressure signal and permeate flow are measured at the permeate stream by a pressure sensor (DRTR-ED, B+B Thermo-Technik GmbH) and a flow meter (Mini CORI-FLOW M14, Bronkhorst Deutschland Nord GmbH), respectively.
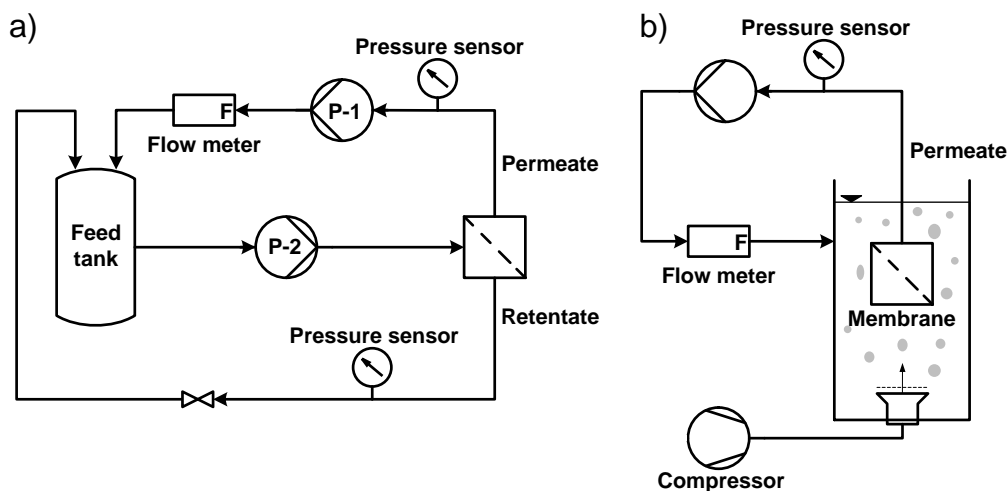
12

Figure 2: Filtration setups used for the impedance measurements: (a) cross-flow filtration cell and (b) immersed dead-end membrane cell.

The second filtration setup consisted of a submerged membrane module which was aerated in order to induce shear and mixing in the feed tank. The reactor where the membrane module was immersed has a volume capacity of 3.3 L. The module was composed of a frame with two flat membranes clamped at both its sides making an effective membrane area of 144 cm^2.

Two different flat sheet ultrafiltration membranes having an active layer made of PES were used in the present study: the LY membrane with a MWCO specification of 100 kDa (Synder Filtration, US), and the UP150 membrane with a MWCO of 150 kDa (Microdyn Nadir, Germany). The membranes were selected to be significantly different in terms of permeabil-

13

ity, fouling behavior and retention properties.

A mixture of different dextran standards (0.5 g/L dextran 40 kDa, 1 g/L dextran 100 kDa and 1 g/L dextran 500 kDa) was used to obtain the experimental MWCO of both membranes. Subsequently, different single standards of selected average molecular weights (2.5 kDa, 100 kDa, and 500 kDa) were used to conduct hydraulic impedance measurements with the LY membrane and correlate the selective properties of the membrane with the corresponding impedance features. Finally, the hydraulic impedance response of both membranes was tested in the submerged filtration cell with solutions of 50 mg/L bovine serum albumin (BSA) and 50 mg/L sodium alginate (NaAlg), both supplied by CarlRoth. The aeration of the submerged cell was not subject of the present study and was kept constant at 0.5 L/min.

The hydraulic impedance measurements were performed by establishing an input function in the permeate pump using the software Dasylab. The input function was created by setting an average flux level to which an additional sine-wave function was added. First, just the average permeate flux was maintained until a steady value of TMP was achieved. Then, the sinusoidal signal having an amplitude of 7 LMH and varying frequencies was implemented. The range of probed frequencies started at 50 mHz and finished at 0.67 mHz; in most of the measurements the same test was performed subsequently using a backwards sequence of frequencies. Both signals, the pressure at the permeate side and the permeate flow rate were registered, treated and analyzed in the frequency domain to obtain the corresponding

14

hydraulic impedance spectrum.

4. Results and discussion

4.1. Correlation between membrane retention and impedance dispersions

Fig. 3 shows the results of the MWCO characterization of the investi-
gated membranes. The intensity of the detector signal corresponding to the
feed and permeate solutions is an estimation of the concentration of dextrans
and, consequently, can be used to calculate the rejection of the membranes
over the range of molecular weights tested [22]. The MWCO is calculated at
the point where a 90 % of rejection is obtained. The values obtained for the
LY and UP membranes are 186 kDa and 1615 kDa, respectively. Such values
differ significantly from the ones specified by the manufacturers, which can
be caused by the different methodologies used by each producer to character-
ize their membranes. Therefore, it is convenient to compare both materials
by using identical experimental procedures. The results obtained clearly in-
dicate that the LY membrane has significantly smaller pore sizes compared
to the UP membrane.

The rejection curve obtained for the LY membrane was taken as a refer-
ence to correlate the rejection properties of ultrafiltration membranes with
their hydraulic impedance response, as this membrane has a tighter distri-
bution of pore sizes compared to the UP membrane. Hydraulic impedance
measurements were conducted with selected dextran standards of average
molecular sizes which would correspond to characteristic degrees of rejec-
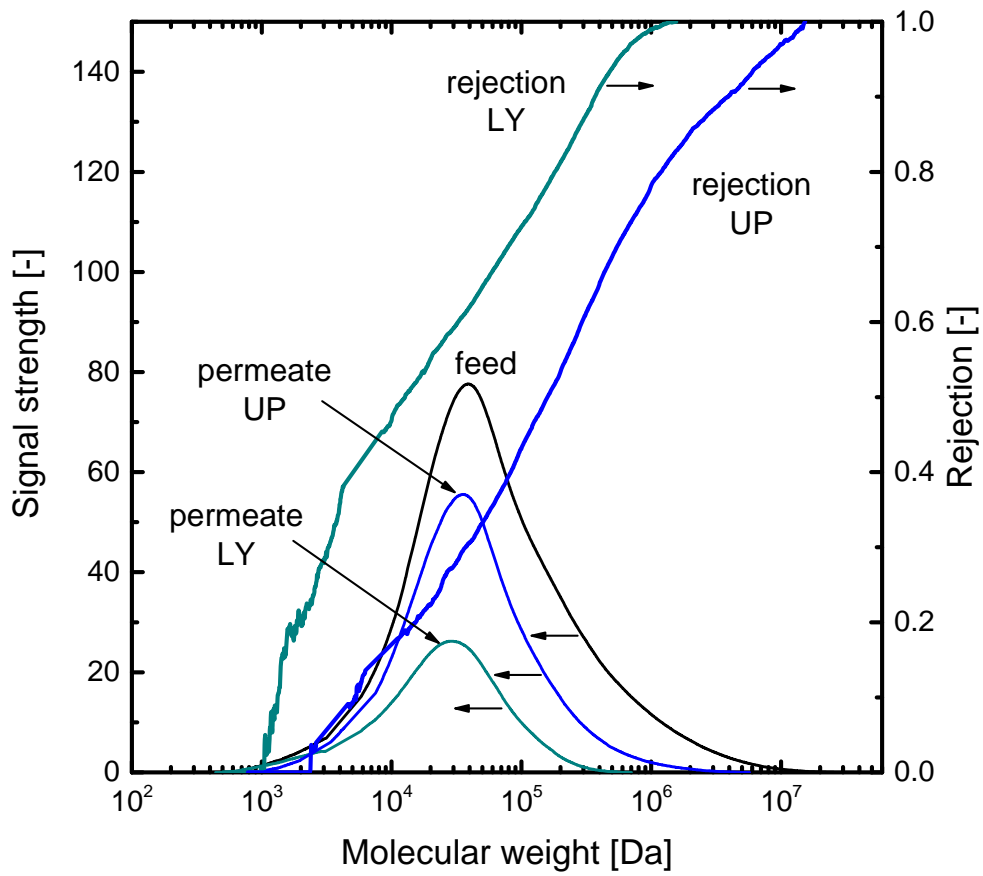
15

Figure 3: SEC plot of dextran concentrations in feed and permeate and rejection curve obtained with both membranes for the experimental determination of their MWCO.

tion by the LY membrane: (a) dextran standard of average molecular size of
2.5 kDa was selected as a system with practically no rejection, (b) dextran
100 kDa was selected as a solute representative for intermediate rejections
and (c) dextran 500 kDa was considered as a system with almost full rejection.

The results obtained with the different dextran standards are shown in
Fig. 4. The system with nearly no rejection (dextran 2.5 kDa) shows the
same behavior as that obtained when filtering distilled water (absence of so-
lutes). Both signals, flux and TMP are in phase over the entire range of
frequencies, thus leading to Nyquist diagrams where the resistance remains
invariant with the frequency. The imaginary component of the impedance,
$Im\,Z_H$, is negligible for the whole range of probed frequencies, whereas the
real impedance, $Re\,Z_H$, takes an almost constant value corresponding to the
inverse of the membrane permeability. This type of response indicates the
absence of any accumulation process in the membrane due to size exclusion
effects. Indeed, the concentration curves obtained for dextran 2.5 kDa (left
side of Fig. 4(c)) show a complete coincidence between permeate and feed
signals correlating with a rejection of 0 %.

According to the MWCO curve shown in Fig. 3, the dextran standard
having an average molecular size of 100 kDa should lie in between the two
extreme cases, where the solutes are partly rejected by the membrane. The
distribution of dextrans in feed and permeate samples collected during the
hydraulic impedance measurements (middle of Fig. 4(c)) is in good agree-
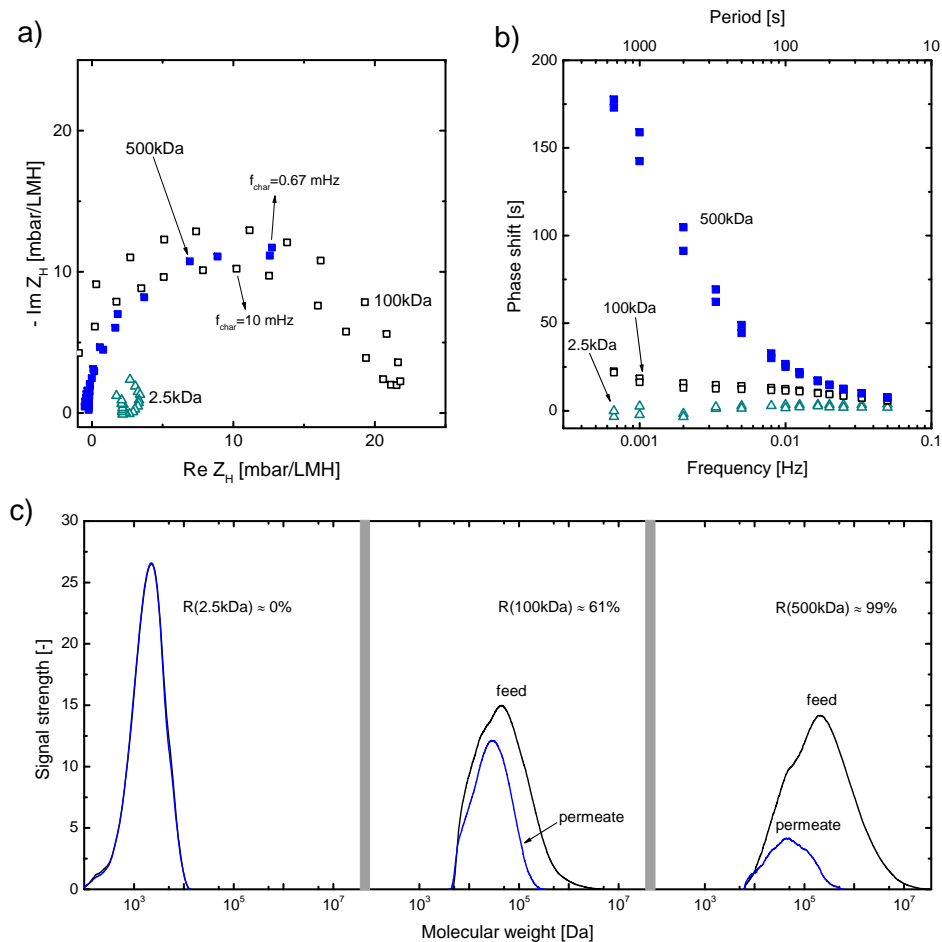ment with this assumption and the membrane cut-off experiments shown

17

Figure 4: Correlation between the impedance response obtained for systems with different rejections. (a) Nyquist plot and (b) Bode plot of the phase shift obtained during the filtration of 2.5 kDa, 100 kDa and 500 kDa dextran standards. (c) Rejection curves obtained from samples taken during the impedance experiments for dextran 2.5 kDa, dextran 100 kDa and dextran 500 kDa.

18

previously. The portion of dextrans of smallest size permeates through the membrane, where both permeate and feed signals overlap. As the molecular size increases, both curves depart from each other and membrane rejection increases correspondingly. The rejection at the average pore size of 100 kDa, close to the maximum peak in the feed curve, takes a value of 61 %. The Nyquist response of this system is analogous to that explained previously in the theoretical section. At very high frequencies, TMP transients do not have enough time to fully develop, which leads to very low values of $Im\, Z_H$ and also very low phase shifts. As the frequency decreases (or analogously, the period T increases), both the amplitude of the TMP signal and the phase shift increase. Accordingly, both $Im\, Z_H$ and $Re\, Z_H$ take higher values and evolve into a semicircle in the Nyquist diagrams. When the frequency of the sinusoidal permeate flux perturbation decreases, the rejected colloids have enough time to accumulate during the ascending phase of a sine cycle and to diffuse back from the membrane surface in the descending phase of each sine cycle, also in an alternating fashion but yet with a significant delay between both signals. Accordingly, the TMP profile becomes broader and a maximum is attained in the Nyquist diagram. The maximum of the semicircle in the Nyquist diagram depicts the frequency at which the system is very close to reaching the steady state. At this range of frequencies, the capacitive-resistive components of the system are equally important, and the amplitude of the TMP will not grow very much by further decreasing the frequency. The inverse of this frequency represents the time constant of the retention process taking place during the ultrafiltration of macromolecules. In other words, the reciprocal of the characteristic frequency indicates how fast foul-

19

ing or concentration polarization layers buildup in the membrane system. As indicated in the plot, the characteristic frequency (f_{char}) takes a value of 10 mHz, which corresponds to a characteristic time of 100 s. Finally, at very low frequencies, the evolution of concentration profiles at the feed side of the membrane takes place almost simultaneously to the variation introduced in the permeate flux signal. In this case, the compliant (i.e. capacitive or cumulative) contribution is negligible compared to the resistive one, and the total hydraulic resistance of the system can be calculated at the intercept with the horizontal axis.

Analyzing the other extreme case, that is the system corresponding with an almost complete rejection (dextran 500 kDa), it can be clearly seen that the TMP response is delayed with respect to the permeate flux. This delay is frequency-dependent and takes very low values at high frequencies, while it increases as the frequency is decreased and the accumulation of colloidal matter becomes significant at the feed side of the membrane (cf. Fig. 4(b)). The response obtained with systems of almost full rejection (see right side of Fig. 4(c)) is quite similar to that observed with solutions which are partially rejected by the membrane. Curiously, in this case, at very low frequencies the Nyquist plot does not converge towards a zero $Im\,Z_H$. Since the amount of rejected dextrans is very high, even when the period of the sinusoidal input signal exceeds 1000 s, the amplitude of TMP still continues increasing and so does the phase shift. This type of behavior may be caused by the accumulation of dextrans of large molecular weight at the feed side needing very long times to reach a steady state thickness of the accumulation layer

20

and because of the very slow back-transport of large species from the vicinity of the membrane towards the bulk solution. Indeed, the maximum in the Nyquist diagram corresponds to a f_{char} of 0.67 mHz, hence to a constant time of 25 minutes. The half semicircle shape of the Nyquist plots is therefore indicating a non-steady deposition of colloids taking place very slowly at the feed side of the membranes. Interestingly, the Nyquist plot obtained for 2.5 kDa and 500 kDa dextrans when a decreasing sequence of frequencies is implemented is identical to that obtained when frequencies are applied in an increasing order. Conversely, the spectrum obtained for 100 kDa dextran exhibits a hysteresis loop. This behavior seems to be related to the fact that the average size of filtered colloids is very similar to the average membrane pore size, thus the accumulation is not happening exclusively at the membrane surface but may involve also internal fouling. An interpretation for such type of behavior will be discussed in more detail below in Section 4.3.

4.2. Hydraulic impedance under membrane-resistance dominant behavior

Once verified that the rejection and accumulation of solutes at the feed side is the main process causing the dispersion between TMP and permeate fluxes, it is not clear yet whether different stages and/or typologies of concentration polarization and fouling can be distinguished through the features obtained in the impedance spectra. Fig. 5(a) shows fouling curves obtained for the UP and LY membrane during the filtration of two typical model foulants, BSA and NaAlg. These curves were obtained from flux-step experiments with the immersed membrane filtration modules (see Fig. 2(b)). The average of the last TMP values registered for every step were then repre-

21

sented against the corresponding permeate flux. The curves obtained for the
UP membrane showcase a behavior typically reported in the literature, where
at low flux values a linear trend of high membrane permeability is observed
[23]. In this region, colloids do not attach to the membrane surface because
back-transport forces are greater than the permeate drag force. Thus, the
membrane resistance is dominating and mainly determines the system perme-
ability. As the flux is increased, a stage of severe fouling is reached, a plateau
is formed in the curves and the flux attains a threshold value. In this case,
the resistance of the accumulation layers developed at the feed side becomes
limiting and the intrinsic membrane resistance is not relevant anymore for
the overall system response. The curves obtained for the LY membrane only
show a slight bending at about 75 LMH with NaAlg solutions. From these
curves, two main facts can be identified: (i) the UP membrane shows a higher
permeability compared with the LY membrane, and (ii) the LY membrane
is less prone to severe fouling according to the quasi-constant permeability
observed over a wide range of permeate fluxes. The latter fact is commonly
found in the literature; many membrane scientists note that higher fluxes of
membranes with higher MWCO can be transitory as they are more suscep-
tible to internal fouling [24–26].

Fig. 5(b) illustrates the TMP evolution during the course of a flux-step
experiment where the step duration was 30 min. In this case, at low per-
meate fluxes the TMP response remains practically constant over the step
duration and rises also in a step-wise fashion. Once the flux reaches 70 LMH,
the pressure is no longer constant and registers an increase over time hav-

22

ing a constant slope. The continuous deposition of rejected matter at the
feed side takes place without reaching a stable TMP value. If flux is further
increased, the fouling rate becomes even higher until a steep boost in TMP
takes place. From both the flux-TMP curves and the flux-step timely evolu-
tion, two different types of membrane behavior can be distinguished: one at
low permeate fluxes where the system response is dominated by the mem-
brane resistance and the TMP reaches steady values, and a second one of
dominating fouling resistance and unsustainable decrease of membrane per-
meability. At this point, it is important to emphasize that, apart from the
fouling rates, no precise information on the type of fouling can be extracted
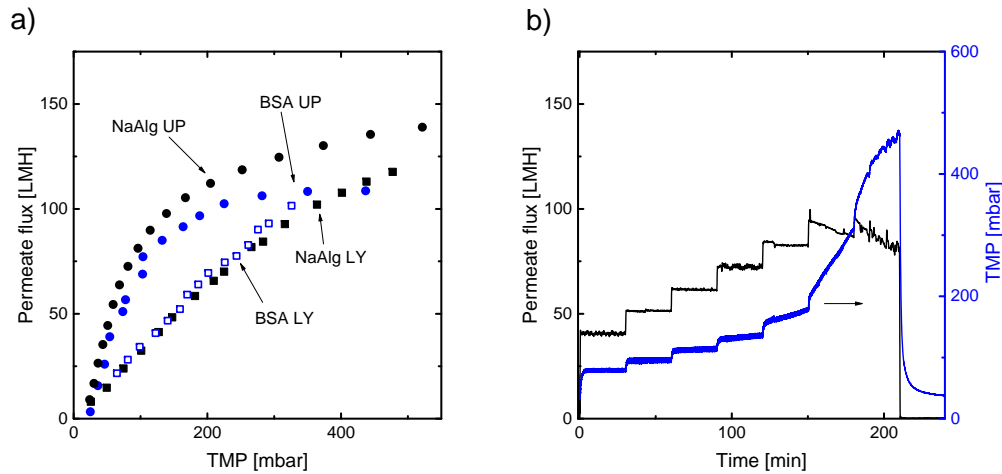from both type of curves shown in Fig. 5.

Figure 5: (a) Flux vs. TMP curves obtained with the UP and LY membranes for 50 mg/L
BSA and 50 mg/L sodium alginate solutions (b) Flux-step experiment performed with the
UP membrane and BSA solutions.

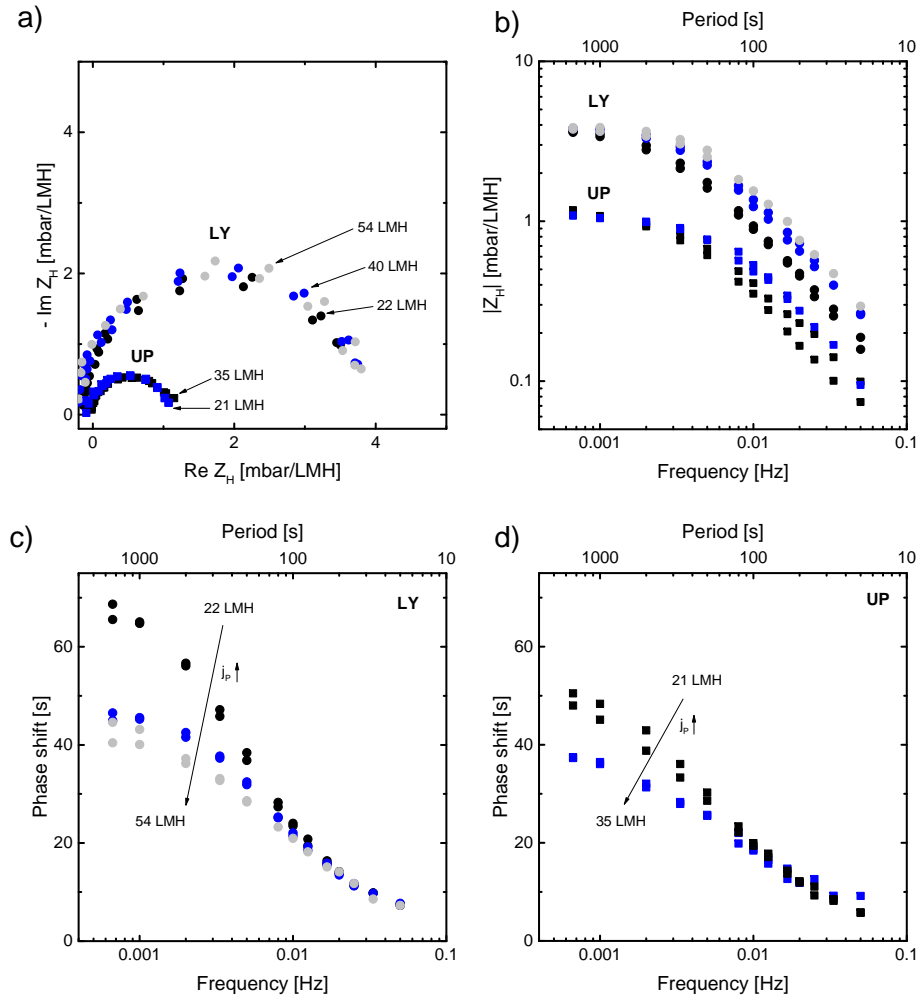Impedance spectra were obtained for the membrane systems at low per-

23

Figure 6: (a) Nyquist plots obtained with BSA solutions with the UP and LY membranes at average permeate fluxes below 60 LMH, (b) corresponding Bode plots of the impedance modulus, and Bode plots of the phase shift obtained for the (c) LY and (d) UP membranes.

meate fluxes, where the intrinsic membrane resistance is dominating (cf. Fig. 6). In these plots only results obtained with BSA are shown, as those registered with NaAlg at low flux levels were very similar. The Nyquist plots obtained with both membranes exhibit a semicircle-shape, which is representative of the combined compliant-resistive behavior previously explained. The notable increase of the imaginary impedance component at intermediate frequencies is a sign of the compliant system behavior caused by the rejection of colloids. Moreover, the real component of the impedance is concomitant to the membrane permeability, as it denotes the resistance to the flow of fluid imposed by the membranes. When the frequency tends to zero, concentration profiles and accumulation layers fully develop simultaneous to the sinusoidal variation in flux (and thus TMP profiles too). Hence, at low frequencies $Im\, Z_H$ tends to zero and the total resistance of the system can be calculated at the intercept of the Nyquist spectra with the x-axis in Fig. 6(a). Besides, it can be clearly seen that the inverse of permeability of both membranes is practically invariant with flux in the region of low permeate fluxes, taking a value of 1.07 and 3.7 mbar/LMH for the UP and LY membrane, respectively. These results are in agreement with the region of constant permeability at low fluxes in the fouling curves of Fig. 5(a). Another remarkable feature of the Nyquist plots is the overlap between the spectra obtained with decreasing and increasing sequence of frequencies.

The Bode plot of the impedance magnitude (Fig. 6(b)) shows the typical behavior of increasing magnitude values as the frequency decreases. At frequencies lower than f_{char}, which in the present case lies around 5 mHz,

25

the response of the system becomes stable and reaches the asymptotic value of the inverse of membrane permeability. The limit of $|Z_H|$ at low frequencies also gives the values of 1.07 and 3.7 mbar/LMH, coinciding with those obtained from the Nyquist plots. Again, the permeability of the LY membrane is clearly lower than that of UP, correlating with the trend previously observed in the fouling curves of Fig. 5(a). With regards to the phase shift, the increase registered when the frequency is decreased from 100 mHz until 6 mHz is generalized and similar for all cases. However, as the frequency becomes smaller than f_{char}, a different steady value is reached depending on the average permeate flux. Curiously, within the regime of under-critical fluxes the phase shift decreases with increasing fluxes. To the contrary, the change in phase shift with flux is not observed in the case of NaAlg systems, as expected. These results seem therefore to be caused by peculiarities of the model foulants rather than by the membranes. A possible explanation for this behavior is the change of conformation that BSA molecules could experience as a consequence of increasing the applied driving force. Interestingly, Howell et al. reported lower rejections during ultrafiltration of BSA at high fluxes, which were attributed to a change in the molecule conformation as a consequence of the increased extensional shear as fluid has to pass faster through the membrane pores [27]. In the present case, rejection of BSA remained unchanged and higher than 90 %. Therefore, an increase in compressibility of rejected BSA seems to be more likely to cause the observed change of phase shift at low frequencies.

26

4.3. Hydraulic impedance under fouling-resistance dominant behavior

Impedance measurements were also conducted at high average fluxes, where the resistance of accumulation layers increases and becomes predominant compared to the intrinsic membrane resistance. The Nyquist plots obtained during the filtration of NaAlg for the UP and LY membrane are presented in Fig. 7(a) and (b), respectively. At the lowest fluxes the spectra have the shape of an almost perfect semicircle, as observed previously in Fig. 6(a). However, as the flux is increased the diameter of the semicircle increases, the spectra become more open and $Im\,Z_H$ does not tend to zero at the limit of low frequencies. This effect is more notorious in the case of the UP membrane, for which the fouling curves also showed a sharp transition from the membrane-resistance to the fouling-resistance dominant region. The open arc registered at high fluxes is analogous to that obtained in our previous publication for mixtures of NaAlg and $CaCl_2$, where an ever-growing gel layer was formed at the top of the membrane [15]. This response is also similar to that shown in Section 4.1 for the filtration of dextran 500 kDa, where rejection was very high. The formation of an alginate gel layer at the feed side of the membrane at high fluxes was observed. This gel layer enhances the compliant behavior of the system, which remains significant at very low frequencies. Thus, the continuous deposition of matter at the gel layer causes the transition from the semicircle to the open arc shape in the Nyquist diagrams.

In contrast with the spectra obtained at low flux levels, where the modulus of the impedance $|Z_H|$ converged to the same value at low frequencies (cf.
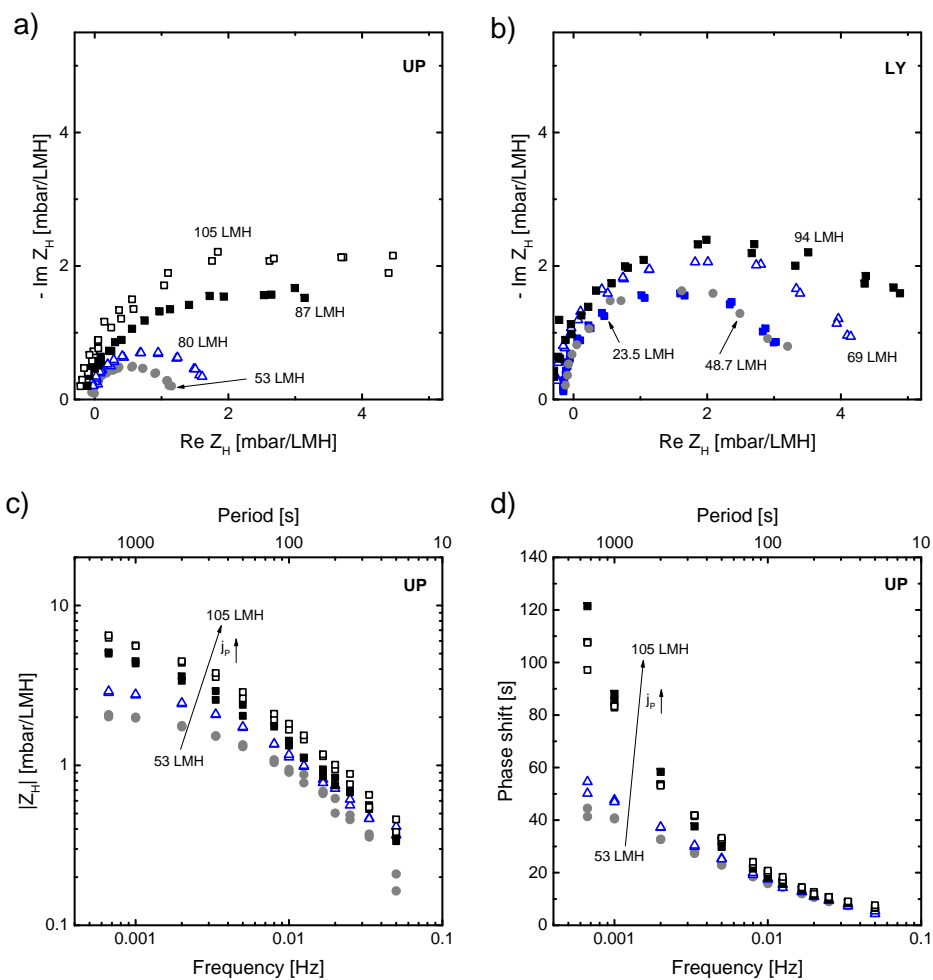
Figure 7: Nyquist plots obtained with 50 mg/L NaAlg at different average flux levels with the (a) UP and (b) LY membrane. Bode plots of the (c) impedance modulus and (d) phase shift corresponding to the impedance measurements carried out with the UP membrane.

Fig. 6(b)), the increase in system resistance with flux can be clearly identified in the Bode diagrams of Fig. 7(c). In addition to this, according to the frequency-dependent evolution of the phase shift at different average fluxes, the flux at which the formation of a gel layer starts to be predominant can be identified in Fig. 7(d). Again, at frequencies higher than 5 mHz the evolution of the phase shift is very similar for all experiments. However, when the frequency decreases further, two differentiated trends can be observed. For the spectra registered at low average fluxes, the maximum phase shift reaches a stable value at low frequencies which lies around 50 s. On the contrary, for fluxes higher than 80 LMH, the phase shift does not reach a stable value and increases further, reaching values even higher than 120s. At high fluxes, an alginate layer is formed on top of the membranes. In this case, for sufficiently low frequencies, additional alginate aggregates have enough time to deposit on top of the already formed gel layer during the rising phase of a sine cycle. As a consequence, the amount of mass accumulated at the feed side increases, thus intensifying the compliant behavior of the system. The delay of TMP with regards to the flux signal boosts accordingly for high fluxes. The obtained results prove that the formation of gel layers can be tracked by evaluating the correlation between phase shift and fluxes at low frequencies. Van de Ven et al. [28] also studied the formation of gel layers by alginates on ultrafiltration membranes and attributed a notable decrease of membrane permeability to the development of gel layers with a very dense structure. Miller et al. also reported a sharp increase in resistance to mass transfer during the ultrafiltration of soybean at fluxes above the threshold flux and pointed out that initiation of cake layer formation was the main
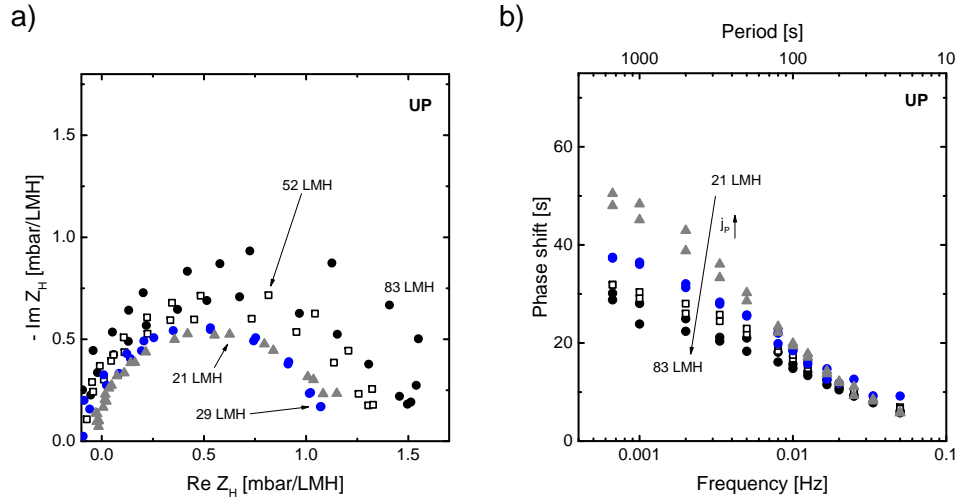
29

Figure 8: Impedance spectra obtained with 50 mg/L BSA at different average flux levels with the UP membrane: (a) Nyquist plots and (b) Bode plots of the phase shift.

reason for such behavior [29]. The formation of initial deposits at constant flux operation is often claimed to cause an increased local flux in the uncovered membrane pores which accelerates gel or cake layer formation. In the present case, the development of a dense alginate gel layer at very high

530 fluxes induces the substantial increase of resistance observed in the fouling curves as well as in the impedance spectra. Therefore, the transition from a membrane-resistance into a fouling-resistance dominated behavior becomes fingerprinted by the changes registered in the impedance spectra.

535 Regarding the effect of sequence of frequencies on the shape of the spectra, both the results obtained at low fluxes (Fig. 6) and at high fluxes with NaAlg solutions (Fig. 7) show no hysteresis. The spectra obtained when high frequencies were first implemented and gradually decreased during the course
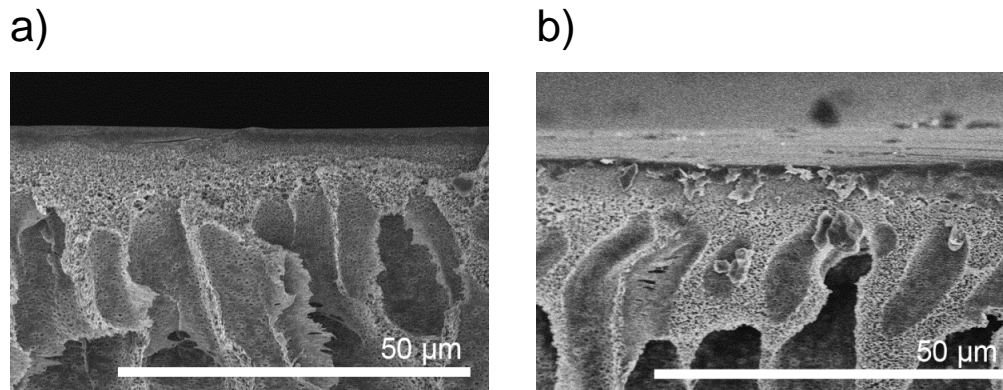
30

Figure 9: SEM pictures of the UP membrane after conducting impedance measurements at fluxes close to the critical with: (a) NaAlg and (b) BSA solutions.

of the experiments overlap with those obtained when reversing the sequence of frequencies (starting from very low frequency values and increasing up to 50 mHz at the end of the experiments). These results indicate that phase shift and amplitude of the corresponding spectra do not rely on the history of the membrane, as concentration polarization and fouling developed during the experiments are reversed back to an initial state when the minimum of the sine perturbation is reached at sufficiently low frequencies. Consequently, in such experiments accumulation of matter is reversible and colloids move back to the bulk when the flux is decreased. Due to the highly reversible character of the accumulation layers, the permeability of the membrane is not altered significantly and a similar response is obtained when a reverse sequence of frequencies is applied.

Differently, the impedance spectra obtained for the UP membrane with BSA solutions at fluxes higher than 50 LMH exhibit a noticeable hysteresis

loop when the order of probed frequencies is reversed (see Fig. 8(a)). The
Nyquist plots registered for decreasing order of frequencies do not overlap
with the plots obtained for increasing order of frequencies. In this case the
state of the membrane is altered and $Im\, Z_H$ as well as $Re\, Z_H$ become higher
when the same type of perturbation signal is applied backwards. Moreover,
hysteresis loops become larger when the flux is further increased from 52 to
83 LMH. The increase in the resistive component ($Re\, Z_H$) denotes a decrease
in membrane permeability. The observed response is explained by the oc-
currence of fouling during the ascending phase of a sine wave which is not
removed when the flux is decreased in a descending phase. Such type of be-
havior can only be caused by an irreversible accumulation process, different
from the formation of reversible gel layers at the membrane surface treated
previously. In this line, the evolution of phase shift with frequency shown in
Fig. 8(b) reveals that, contrary to the formation of alginate gel layers, the
jump in phase shift at high fluxes characteristic of dense blocking layers is not
manifested in the case of BSA. Consequently, hysteresis loops denote the evo-
lution of internal fouling and not at the membrane surface. The application
of very high fluxes seems to push BSA molecules into the porous membrane
network. When a molecule or aggregate of BSA molecules is deposited inside
a pore, it blocks a path for the permeation of water and thus decreases the
membrane permeability. The settling and entrapment of BSA in the pores
can be difficultly removed by decreasing the flux, which would explain the
hysteresis loops. The response obtained for the UP membrane and BSA so-
lutions at high fluxes is homologous to that shown previously in Section 4.1
during the filtration of dextrans with a size similar to the pores width. The

32

formation of internal deposits and accumulation of BSA inside the pores of the UP membrane was visualized in SEM pictures. Fig. 9 shows two SEM pictures of the cross section of the UP membrane after the filtration of NaAlg and BSA at fluxes higher than 50 LMH. In the case of NaAlg, the formation of a gel layer acts as an additional resistance which is selective to the permeation of more NaAlg molecules through the membrane. However, when BSA was filtered the development of internal irreversible fouling was verified.

It is also remarkable that the flux level at which the evolution of internal fouling is detected in the fluidic impedance spectra (52 LMH) is considerable lower than the value at which the bending in the j_P-TMP curve of Fig. 5(a) becomes noticeable. Also, the timely TMP evolution registered at 50 LMH for the same system in Fig. 5(b) during a flux-step experiment does not show signs of detrimental fouling phenomena, as TMP remains practically constant. A significant fouling rate $dTMP/dt$ does not start to be noticeable until a flux of 70 LMH is imposed. However, fouling rates do not provide information about the class of fouling taking place. The different results obtained for both membrane-resistance and fouling-resistance dominated behavior highlight the valuable information that can be gained from hydraulic impedance spectroscopy. It is evident that important fouling phenomena can take place at fluxes considerable lower than those predicted from conventional constant pressure or constant flux measurements, whereas they can be easily tracked in impedance diagrams. The evolution of phase shift dispersions with the values of average permeate flux allow identifying the formation of gel layers on top of a membrane surface, while hysteresis loops in the Nyquist

33

plots for reversed sequences of probed frequencies trace the development of irreversible fouling. Nir et al. were also able to distinguish internal fouling from gel layer formation at the surface of microfiltration membranes by means of using electrochemical impedance spectroscopy [30]. The outcomes of the present work are not only applicable to get further insight in the fundamental phenomena related to fouling in pressure-driven membrane processes but could be also implemented for the early diagnosis of irreversible fouling during industrial applications of membrane processes. Sine-wave functions at very low frequency can be periodically programmed during the normal operation of a membrane system in order to obtain a fast recognition of critical fouling events, which would allow taking timely actions to recover membrane permeability (i.e. performing a backwash or chemical cleaning) before a fast degradation of the membrane becomes unavoidable.

5. Conclusions

The evolution of distinct fouling phenomena in ultrafiltration was studied under conditions of constant average permeate fluxes by conducting hydraulic impedance spectroscopy measurements. The potential and sensitivity of this technique has been explored with the aim of identifying the nature of fouling processes taking place in different membrane/foulant systems. First the correlation between the compliance of membrane systems and their selective properties is demonstrated, as the registration of TMP signals which are out of phase with the respective j_P signals occurs only with systems where colloids are significantly rejected. Then, different characteristic features appearing in impedance spectra have been linked to specific fouling

34

events influencing the overall hydraulic resistance of membrane systems:

(i) At under-critical fluxes the perfect semicircle shape obtained in the Nyquist diagrams showcases that the intrinsic membrane resistance mainly determines the system's resistance and permeability. The semicircle is representative for the compliant behavior concomitant to the rejection of colloids as well as for the permeance of solvent through the membranes.

(ii) As the flux is increased and gel layers are formed on top of the membrane surface, the semicircle in the Nyquist diagram becomes more open and bigger. This effect marks the point at which the contribution of accumulation layers to the hydraulic resistance starts to become relevant and more limiting than the intrinsic membrane resistance. This effect is specially visible when NaAlg solutions are investigated.

(iii) The overlapping of impedance spectra regardless of the sequence of probed frequencies (increasing or decreasing) showcases the reversibility of fouling. On the contrary, hysteresis loops are characteristic of systems where internal irreversible fouling occurs. The latter has been verified during the filtration of BSA with a membrane with a broad distribution of pore sizes.

In conclusion, hydraulic impedance spectroscopy has been demonstrated to be a powerful and highly informative technique to reveal the nature and intensity of fouling taking place in ultrafiltration processes. Apart from potential applications to investigate physical phenomena in membrane filtration, we claim that this method can be systematically applied to anticipate the development of critical fouling in membrane processes and apply appropriate

35

countermeasures to prevent it.

Acknowledgments

References

[1] W. Chen, C. Qian, W. L. Hong, J. X. Cheng, H. Q. Yu, Evolution of membrane fouling revealed by label-free vibrational spectroscopic imaging, Environ. Sci. Technol. 51 (2017) 9580–9587.

[2] M. C. Martí-Calatayud, M. C. Vincent-Vela, S. Álvarez-Blanco, J. Lora-García, E. Bergantiños-Rodríguez, Analysis and optimization of the influence of operating conditions in the ultrafiltration of macromolecules using a response surface methodological approach, Chem. Eng. J. 156 (2010) 337–346.

[3] H. B. Park, J. Kamcev, L. M. Robeson, M. Elimelech, B. D. Freeman, Maximizing the right stuff: The trade-off between membrane permeability and selectivity, Science 356 (2017) 1138–1148.

[4] P. Bacchin, P. Aimar, V. Sanchez, Model for colloidal fouling of membranes, AIChE J. 41 (1995) 368–376.

[5] R. W. Field, D. Wu, J. A. Howell, B. B. Gupta, Critical flux concept for microfiltration fouling, J. Membr. Sci. 100 (1995) 259–272.

[6] J. Lohaus, Y. M. Perez, M. Wessling, What are the microscopic events of colloidal membrane fouling?, J. Membr. Sci. 553 (2018) 90–98.

[7] W. Zhang, J. Luo, L. Ding, M. Y. Jaffrin, A review on flux decline control strategies in pressure-driven membrane processes, Ind. Eng. Chem. Res. 54 (2015) 2843–2861.

[8] R. W. Field, G. K. Pearce, Critical, sustainable and threshold fluxes for membrane filtration with water industry applications, Adv. Colloid Interf. Sci. 164 (2011) 38–44.

[9] P. Bacchin, P. Aimar, R. W. Field, Critical and sustainable fluxes: Theory, experiments and applications, J. Membr. Sci. 281 (2006) 42–69.

[10] B. Espinasse, P. Bacchin, P. Aimar, Filtration method characterizing the reversibility of colloidal fouling layers at a membrane surface: Analysis through critical flux and osmotic pressure, J. Colloid Interf. Sci. 320 (2008) 483–490.

[11] P. van der Marel, A. Zwijnenburg, A. Kemperman, M. Wessling, H. Temmink, W. van der Meer, An improved flux-step method to determine the critical flux and the critical flux for irreversibility in a membrane bioreactor, J. Membr. Sci. 332 (2009) 24–29.

[12] P. Le-Clech, V. Chen, T. A. G. Fane, Fouling in membrane bioreactors used in wastewater treatment, J. Membr. Sci. 284 (2006) 17–53.

[13] M. Remy, P. van der Marel, A. Zwijnenburg, W. Rulkens, H. Temmink, Low dose powdered activated carbon addition at high sludge retention times to reduce fouling in membrane bioreactors, Water Res. 43 (2009) 345–350.

[14] J. A. Gil, E. Dorgeloh, J. B. van Lier, J. H. J. M. van der Graaf, D. Prats, Start-up of decentralized MBRs. Part I: The influence of operational parameters, Desalination 285 (2012) 324–335.

[15] M. C. Martí-Calatayud, M. Wessling, Hydraulic impedance spectroscopy tracks colloidal matter accumulation during ultrafiltration, J. Membr. Sci. 535 (2017) 294–300.

[16] L. N. Sim, J. Gu, H. G. Coster, A. G. Fane, Quantitative determination of the electrical properties of RO membranes during fouling and cleaning processes using electrical impedance spectroscopy, Desalination 379 (2016) 126–136.

[17] F. Roghmans, M. C. Martí-Calatayud, S. Abdu, R. Femmer, R. Tiwari, A. Walther, M. Wessling, Electrochemical impedance spectroscopy fingerprints the ion selectivity of microgel functionalized ion-exchange membranes, Electrochem. Commun. 72 (2016) 113–117.

[18] T. C. Chilcott, A. Antony, G. Leslie, In situ electrical impedance characterization of fouling by calcium agents in reverse osmosis membrane

systems using Maxwell Wagner and hydrodynamic models, Desalination

720   403 (2017) 64–79.

[19] B. J. Kirby, Hydraulic Circuit Analysis, in: Micro- and nanoscale fluid mechanics. Transport in microfluidic devices, Cambridge University Press, New York, 2010, Ch. 3, pp. 60–78.

[20] L. H. Moleiro, M. Mell, R. Bocanegra, I. López-Montero, P. Fouquet,

725   T. Hellweg, J. L. Carrascosa, F. Monroy, Permeability modes in fluctuating lipid membranes with DNA-translocating pores, Adv. Colloid Interface Sci. 247 (2017) 543–554.

[21] H. Bruus, Theoretical microfluidics, Oxford University Press, Oxford, 2008.

730 [22] C. Fritzmann, M. Wiese, T. Melin, M. Wessling, Helically microstructured spacers improve mass transfer and fractionation selectivity in ultrafiltration, J. Membr. Sci. 463 (2014) 41–48.

[23] H.-D. Park, I.-S. Chang, K.-J. Lee, Principles of membrane bioreactors for wastewater treatment, CRC Press; IWA Publishing, Boca Raton FL,

735   2015.

[24] R. W. Baker, Membrane technology and applications, John Wiley & Sons, Inc., 2004.

[25] K. Zeng, J. Zhou, Z. Cui, Y. Zhou, C. Shi, X. Wang, L. Zhou, X. Ding, Z. Wang, E. Drioli, Insight into fouling behavior of poly(vinylidene fluo-

740   ride) (PVDF) hollow fiber membranes caused by dextran with different pore size distributions, Chin. J. Chem. Eng. 26 (2017) 268–277.

[26] B. Tansel, N. Dizge, I. N. Tansel, Analysis of high resolution flux data to characterize fouling profiles of membranes with different MWCO under different filtration modes, Sep. Purif. Technol. 173 (2017) 200–208.

[27] J. A. Howell, D. Wu, R. W. Field, Transmission of bovine albumin under controlled flux ultrafiltration, J. Membr. Sci. 152 (1999) 117–127.

[28] W. J. C. van de Ven, K. van't Sant, I. G. M. Pünt, A. Zwijnenburg, A. J. B. Kemperman, W. G. J. van der Meer, M. Wessling, Hollow fiber dead-end ultrafiltration: Influence of ionic environment on filtration of alginates, J. Membr. Sci. 308 (2008) 218–229.

[29] D. J. Miller, S. Kasemset, D. R. Paul, B. D. Freeman, Comparison of membrane fouling at constant flux and constant transmembrane pressure conditions, J. Membr. Sci. 454 (2014) 505–515.

[30] O. Nir, T. Trieu, S. Bannwarth, M. Wessling, Microfiltration of deformable microgels, Soft Matter 12 (2016) 6512–6517.